



Continuous syntheses of Pd@Pt and Cu@Ag core-shell nanoparticles using microwave-assisted core particle formation coupled with galvanic metal displacement

Journal:	<i>Nanoscale</i>
Manuscript ID:	NR-ART-01-2014-000118.R2
Article Type:	Paper
Date Submitted by the Author:	23-Apr-2014
Complete List of Authors:	Miyakawa, Masato; National Institute of Advanced Industrial Science and Technology, AIST, Hiyoshi, Norihito; National Institute of Advanced Industrial Science and Technology, AIST, Nishioka, Masateru; National Institute of Advanced Industrial Science and Technology, AIST, Koda, Hidekazu; Shinko-Kagaku Co. Ltd., Sato, Koichi; National Institute of Advanced Industrial Science and Technology, AIST, Miyazawa, Akira; National Institute of Advanced Industrial Science and Technology, AIST, Suzuki, Toshishige; Research Center for Compact Chemical Process, National Institute of Advanced Ind, Research Center for Compact Chemical Processes

Continuous syntheses of Pd@Pt and Cu@Ag core–shell nanoparticles using microwave-assisted core particle formation coupled with galvanic metal displacement

Masato Miyakawa,^{*a} Norihito Hiyoshi,^a Masateru Nishioka,^{*a}

Hidekazu Koda,^b Koichi Sato,^a Akira Miyazawa,^a

and Toshishige M. Suzuki^a

^a*National Institute of Advanced Industrial Science and Technology, AIST,
4-2-1, Nigatake, Miyagino-ku, Sendai, 983-8551, Japan*

^b*Shinko-Kagaku Co. Ltd.*

1544-19, Mashimori, Koshigaya-shi, Saitama, 343-0012, Japan

E-mail: masato-miyakawa@aist.go.jp, m-nishioka@aist.go.jp

Abstract

Continuous synthesis of Pd@Pt and Cu@Ag core–shell nanoparticles was performed using flow processes including microwave-assisted Pd (or Cu) core–nanoparticle formation followed by galvanic displacement with a Pt (or Ag) shell. The core–shell structure and the nanoparticle size were confirmed using high-angle annular dark-field scanning transmission electron microscopy (HAADF-STEM) observation and EDS elemental mapping. The Pd@Pt nanoparticles with particle size of 6.5 ± 0.6 nm and Pt shell thickness of ca. 0.25 nm were synthesized with appreciably high Pd concentration (Pd 100

mM). This shell thickness corresponds to one atomic layer thickness of Pt encapsulating the Pd core metal. The particle size of core Pd was controlled by tuning the initial concentrations of $\text{Na}_2[\text{PdCl}_4]$ and PVP. Core-shell Cu@Ag nanoparticles with particle size of 90 ± 35 nm and Ag shell thickness of ca. 3.5 nm were obtained using similar sequential reactions. Oxidation of the Cu core was suppressed by the coating of Cu nanoparticles with the Ag shell.

Introduction

The physical and chemical properties of metal nanoparticles improve drastically by encapsulation with other appropriate metals.¹⁻⁸ In addition, the cost of precious metal nanoparticles can be reduced by using inexpensive core metals while maintaining characteristics of the outer shell metal. Moreover, shell metal layers prevent the oxidation of core metals. Therefore corrosion and leaching of core metals are also suppressed. Pd@Pt core-shell nanoparticles have attracted remarkable attention for use as electrode materials of polymer electrolyte membrane fuel cells (PEMFC) because of their considerably enhanced oxygen reduction activity compared to a Pt catalyst when used alone without the core-shell structure.⁹⁻²⁰

The uses of silver nanoparticles for electronic devices, conductive coatings and metal inks for inkjet printing have been known for years.²¹⁻²³ In fact, Cu nanoparticles have been regarded as an alternative to Ag not only for economic reasons but also because Cu possesses high electrical conductivity comparable to that of Ag. Nevertheless, the easy oxidation of Cu strongly limits its use as an Ag substitute. Protection of Cu nanoparticles with an Ag

shell i.e., core–shell Cu@Ag, has been regarded as an alternative method to prevent spontaneous Cu oxidation.^{24–28}

Among the various methods, wet-chemical processes have been widely accepted for core–shell nanoparticle syntheses.^{1, 3–18, 20, 24–28} Earlier studies of Pd@Pt and Cu@Ag syntheses involved multiple steps of batch procedures such as separation, washing, and pre-treatment of core metal nanoparticles and subsequent coating procedures of metal shells. Moreover, chemicals such as reducing agents, surface modification reagents, and surfactants are frequently used.

Flow-type processes generally present advantages over batch processes with respect to continuous material production. Microwave (MW) dielectric heating has been used for inorganic/organic syntheses^{29–37} and metal nanoparticle synthesis.^{38–40} We originally designed an MW flow reactor system that forms a uniform electromagnetic field in a cylindrical single-mode MW cavity.^{41–43} A homogeneous heating zone can be created with certainty in the reactor tube mounted along the central axis of the MW cavity. Continuous flow synthesis of metal nanoparticles and metal complexes in polyols has been achieved using our MW reactor systems at ambient pressure and at elevated pressure.^{41–43}

For this study, we attempted to conduct a series of reactions coherently in a flow reactor system, i.e., MW-assisted flow reaction for rapid synthesis of core Pd (or Cu) nanoparticles with subsequent direct coating of Pt (or Ag) shell by the galvanic replacement reaction. In this system, spontaneous oxidation of core nanoparticles can be avoided by the direct transfer of a core metal

dispersion into a shell formation reaction without isolation. Moreover, specific chemicals are not necessary. The structure, particle size, and distribution of metals in Pd@Pt and Cu@Ag particles were characterized by HAADF-STEM observations and EDS elemental mapping. Suppression of Cu oxidation by coating with an Ag shell was evaluated using UV-vis absorption spectra.

Experimental

Chemicals

For use in this study, Na₂[PdCl₄] (98%) and poly(*N*-vinylpyrrolidone) (PVP, Mw = 10,000) were purchased from Aldrich Chemical Co. Inc. Also, Cu(OAc)₂ (97%) (OAc=acetate), H₂[PtCl₆]·6H₂O (98.5%), AgNO₃ (98%), NaOH (97%), ethylene glycol (EG), and glycerol were purchased from Wako Pure Chemical Industries Ltd.

Microwave reactor system

The MW reactor system consists of a variable-frequency microwave generator (2.5 GHz ± 200 MHz, 100 W) and a cylindrical single-mode cavity.^{41, 43} The inner diameter of TM₀₁₀ single-mode cavity was designed based on the incident electromagnetic wave frequency (2.45 GHz). The cavity length was 100 mm. A quartz tubular reactor (ID 1 mm) used as the flow-type reactor was mounted coaxially in the center of the TM₀₁₀ cavity. The oscillation frequency for matching with the resonance frequency was monitored. The applied power was controlled by the temperature feedback module. This MW reactor system

is useful for rapid heating of liquid flows at pressures up to 10 MPa. The temperature of the reaction is measured using a radiation thermometer through the open slit (8 mm width) of the cavity.

Flow synthesis of Pd@Pt and Cu@Ag core-shell nanoparticles

A schematic view of the process developed for the continuous synthesis of metal@metal core-shell nanoparticles is portrayed in Fig. 1. Core nanoparticles were synthesized with a MW-assisted polyol process using either EG or glycerol as the reaction medium. An EG solution containing $\text{Na}_2[\text{PdCl}_4]$ (100 mM) as a metal precursor and PVP (15 wt%) as a stabilizing agent was introduced continuously into the quartz tube reactor placed in the center of the microwave cavity. Actually, EG works as the reaction solvent and the reducing agent. Because of the high dielectric constant, polyols such as EG and glycerol efficiently convert MW energy to thermal energy. EG (bp 195 °C) was heated to 200 °C using MW irradiation under application of pressure. The microwave heating temperature was set at 200 °C with the flow rate of 50 ml h^{-1} which corresponds to residence time of 6 s. The reaction fluid was pressurized using a pump (Nanospace SI-2; Shiseido Co. Ltd.). The pressure was controlled manually using a pressure regulator. The solution was transferred directly to the T-type mixer for a metal-shell coating process without particle isolation. Preparation of Pd nanoparticles having different sizes was conducted by changing the concentrations of $\text{Na}_2[\text{PdCl}_4]$ and PVP.

The Pd nanoparticle dispersion was mixed with a Pt shell precursor solution ($\text{H}_2[\text{PtCl}_6] \cdot 6\text{H}_2\text{O}$ (100 mM) in EG). Then the solution pH was

adjusted with 5 M aqueous NaOH solution at the second T-mixer. The molar ratio of Pd : Pt was 3 : 1 and the pH value of the NaOH solution after mixing was controlled to 12. Then the reaction mixture was taken out of the mixer and let to stand at room temperature (6–72 h) for the Pt shell growth by a galvanic displacement reaction.

Core-shell nanoparticles of Cu@Ag were synthesized in a procedure similar to that of Pd@Pt using Cu(OAc)₂ and AgNO₃ as the respective precursors of core and shell metals. A mixed solution of 10 mM Cu(OAc)₂ and 3 wt% PVP dissolved in glycerol was introduced continuously to the MW reactor (200 °C; reaction time 30 s) for the preparation of Cu core nanoparticles. Then AgNO₃ (10 mM) and NaOH (300 mM) dissolved in EG were mixed to the Cu nanoparticle dispersion. The molar ratio of Cu : Ag was 6 : 1. The pH value after mixing of NaOH solution was adjusted to 9. The reaction mixture was finally left standing at room temperature for 24 h. Nanoparticles of Pd@Pt and Cu@Ag were separated from the reaction solution by centrifugation and were again dispersed with ethanol and provided for TEM, HAADF-STEM, and EDS analysis, and for UV-vis spectral measurements.

Instruments

The sizes and distribution of nanoparticles were determined using transmission electron microscopy (TEM, TECNAI G2; FEI Co.) images. TEM samples were prepared by dropping nanoparticle dispersions onto a carbon film supported by the Cu or Mo grids. High-angle annular dark-field scanning

transmission electron microscopy (HAADF-STEM) and energy dispersive X-ray spectrometry (EDS) analysis of Pd@Pt core-shell nanoparticles were done (JEM-ARM200F; JEOL Ltd.). An EDS mapping image of Cu@Ag core-shell nanoparticles was obtained (JEM-2200FS; JEOL Ltd.). The UV-vis absorption spectra of nanoparticle dispersions were recorded using a spectrophotometer (U-3310; Hitachi Ltd.).

Results and Discussion

Palladium nanoparticles of 6.5 nm average size (standard deviation of 0.6) were obtained continuously in 6 s of residence time in the MW heated reactor zone at 200 °C (Fig. S1). In contrast, as TEM image and UV-vis spectra show, the formation of nanoparticles of homogeneous size was unfavorable at 160 °C (Fig. S1). The solution temperature rose instantaneously, reaching the setting temperature (200 °C) in a few seconds. This temperature was maintained with high precision (± 1 °C).^{41, 43} Rapid heating to high temperatures produced the narrow size distribution of Pd nanoparticles because of homogeneous nucleation and subsequent crystal growth. The Pd particle size can be controlled by tuning the concentration of Na₂[PdCl₄] and PVP within the range of ca. 3–11 nm (Fig. S2). The Pd particle size increased as the initial concentration of Na₂[PdCl₄] solution increased, while PVP functions as the capping agent of Pd particle and suppresses the particle growth.

For the Pt shell formation, the Pd nanoparticle (6.5 nm) dispersion was mixed with H₂[PtCl₆]·6H₂O solution with the molar ratio of Pd : Pt = 3 : 1. Then pH was adjusted at 12. Fig. 2 shows the HAADF-STEM image and line

profile of Pd@Pt core-shell nanoparticles. The Z value of Pt ($Z = 78$) and Pd ($Z = 46$) is appreciably different. Therefore, the nanoparticle structure can be determined by the contrast of the image. The Z -contrast image in Fig. 2 shows brighter shells over a darker nanoparticle, indicating the formation of Pd@Pt core-shell structure. Nanoparticles of 6.5 ± 0.6 nm were observed in the TEM image shown in Fig. S3. This particle size was similar to that of the started Pd core nanoparticle. Elemental mapping images presented in Fig. 3 confirm the uniform encapsulation of Pd core by the Pt shell; Pt is abundant at the surface and surrounds the dense Pd core. Based on the atomic ratio (Pd : Pt = 87 : 13) determined using EDS analysis, the shell thickness was estimated as ca. 0.25 nm. This value corresponds to one atomic layer thickness of Pt encapsulating the Pd core metal.^{9,20} In an earlier report, Pd@Pt nanoparticles of ca. 7 nm with sub-1 nm Pt shell thickness were described as suitable for practical use as a PEM fuel cell catalyst.²⁰ Further growth of Pt shell was not observed by increase of the Pt ratio against Pd. For example, when the molar ratio of Pt was increased from Pd : Pt = 3 : 1 to 2 : 1, the shell thickness did not change. Instead, the abundance of free Pt nanoparticles increased in the bulk solution. Fig. S4 portrays the time dependence of atomic mapping images during the galvanic replacement reaction by leaving 6 h, 24 h, and 72 h at room temperature. Particle sizes and the atomic ratio (Pd : Pt = 87 : 13) did not change to any great degree after standing for 6 h, suggesting that the shell growth was completed within 6 h and that it was stable thereafter. Actually, the core-shell structure is very stable. The particle size remained unchanged for six months during storage in ethanol (Fig. S5). The sizes of Pd@Pt core-shell nanoparticles are

controllable because the Pd particle size can be controlled by tuning the concentrations of Pd precursor and the capping agent.

The galvanic replacement reaction is driven by the difference of redox potentials between the core metal and the metal ion in the solution. In the present system, oxidation of the core Pd surface is accompanied by the reduction of the outer metal ion, i.e. $[\text{PtCl}_6]^{2-}$. The alkaline condition is necessary for the Pt shell formation. Fig. 4 shows that the formation of a distinct Pt shell was unlikely unless pH was controlled to alkaline.¹⁸ In contrast metal–metal displacement took place at pH 12, even at room temperature. In a separate experiment, we added $\text{H}_2[\text{PtCl}_6]$ to Pd nanoparticles dispersed EG solution adjusted at different pH. The sharp absorption peak of $[\text{PtCl}_6]^{2-}$ at 270 nm gradually disappeared in alkaline conditions (pH 12), although the change of the peak intensity was extremely slight at pH 7 (Fig. S6). This observation suggests that the base hydrolysis of $[\text{PtCl}_6]^{2-}$ took place in alkaline media yielding a Pt-hydroxide complex. An X-ray absorption study of the controlled synthesis of Ru@Pt confirmed that $[\text{PtCl}_6]^{2-}$ in EG solution changes to $[\text{Pt}(\text{OH})_4]^{2-}$ at pH 12 by reduction of Pt(IV) to Pt(II) and ligand exchange from Cl^- to OH^- .⁴⁴ Then galvanic replacement with the Ru cluster occurred easily. Similarly, $[\text{Pt}(\text{OH})_4]^{2-}$ formed at pH 12 can be responsible for the easy metal displacement with Pd core at high pH, as observed in this study. At extremely high pH (>13), however, nucleation and growth of free Pt nanoparticles in the bulk solution were enhanced in place of core–shell formation. As a result, a mixture of Pd@Pt and Pt nanoparticles was formed (Fig. S7).

To verify the versatility of our MW-assisted flow reaction and *in-situ*

shell formation, we demonstrated the synthesis of Cu@Ag core-shell nanoparticles. The main difficulty of Cu nanoparticles arises from their easy oxidation during their synthesis, which takes an extremely long time. The MW-assisted polyol process enables rapid Cu core formation. Subsequent wrapping of Cu nanoparticles by the Ag shell might contribute greatly to the resistance of Cu core to get oxidized. Fig. 5 shows TEM images and EDS mapping images of Cu and Cu@Ag core-shell nanoparticles. The particle sizes determined from TEM images of Cu and Cu@Ag core-shell nanoparticles were, respectively, 89 ± 34 nm and 90 ± 35 nm. The distribution of Cu and Ag atoms along the cross section line (Fig. 5c) suggests the formation of a uniform Ag shell over the surface of the Cu nanoparticle. The Ag shell thickness was estimated as ca. 3.5 nm from the atomic ratio (Cu : Ag = 85 : 15) determined using EDS analysis. The pH of dispersed solution is an important factor for preferential Ag deposition on the Cu core. Figs. S8(a) and S8(b) show TEM images of nanoparticles after standing for 24 h at pH 10 and 11, respectively. For pH 10, large nanoparticles (50–200 nm) and small nanoparticles (5–10 nm) were mixed, but only small nanoparticles were observed at pH 11. UV-vis spectra (Fig. S8(c)) of the dispersion prepared at pH 10 yielded two peaks associated with Cu (600 nm) and Ag (400 nm) plasmon absorption bands, but at pH 11, only the absorption of Ag nanoparticles was observed. The surface of dispersed metal particles is equilibrated with M-OH and M-O⁻ depending on the pH relative to the pK_a value of the hydroxylated metal surface.⁴⁵ At high pH, the surface will be more negative according to the increase of M-O⁻ promoted by proton dissociation. A

similarly negative charge of Cu surface will be dominant with increased pH, which enhances the access of Ag^+ and facilitates the galvanic replacement. However, this shell formation reaction competes with the nucleation and growth of Ag nanoparticles in the bulk solution, particularly in a high pH environment because the reducing strength of polyols tends to increase as pH increases.⁴⁶ A very high pH condition ($\text{pH} > 11$) causes formation of bare Ag nanoparticles in the bulk solution by the polyol reduction,⁴⁷ which reduces the Ag^+ concentration in bulk solution. The opportunities for core-shell nanoparticle formation decrease.

Fig. 6 presents the time course of UV-vis spectra of (a) Cu nanoparticle dispersion and (b) Cu@Ag nanoparticle dispersion upon standing at room temperature. The spectra of the as-prepared Cu samples (Fig. 6a) showed characteristic absorption peaks at around 600 nm associated with the plasmon resonance band of Cu nanoparticles. The peak intensity decreased with time and finally almost disappeared after 1 day, suggesting that rapid oxidation and dissolution of Cu took place.²⁴ In fact, only a few Cu nanoparticles with 15 nm maximum size were found using TEM measurements (Fig. S9a). A broad peak (ca. 400 nm) other than the 600 nm peak was observed in the Cu@Ag dispersion (Fig. 6b), assignable to the Ag plasmon resonance absorption. Contrary to bare Cu nanoparticles, the reduction of Cu peak intensity in Cu@Ag dispersion was slow because the Cu core surface is protected by an Ag shell layer. Although the size and shape were irregular, Cu@Ag nanoparticles remained undissolved after standing 7 days in ethanol (Fig. S9b), indicating the longer life of the core-shell structure.

Conclusions

Continuous synthesis of metal@metal core-shell nanoparticles was demonstrated by integration of a series of reactions including MW-assisted polyol process for core metal nanoparticle formation followed by coating with different metal shells. Core metal particles (Pd, 6.5 nm; Cu, 90 nm) were synthesized rapidly and continuously using homogeneous MW heating and precise temperature control. The shell formation reaction by galvanic metal replacement was influenced by the pH of the solution used for the shell formation. Coating of a sub-1 nm Pt shell over Pd core was attained at pH 12, where $[\text{Pt}(\text{OH})_4]^{2-}$ is apparently involved as a reaction intermediate. Approximately pH 9 was the most favored region for Ag shell formation on the Cu core. When pH exceeds 11, Cu core particles disappeared; only Ag nanoparticles were formed. Enhanced durability of oxidation-sensitive Cu nanoparticles was realized by protection with the Ag shell. This flow reactor system is a promising candidate for use in continuous production of metal@metal core-shell nanoparticles.

Acknowledgements

We are grateful to the Bio-Nano Electronics Research Centre of Toyo University supporting TEM analysis (JEM-2200FS; JEOL Ltd.).

Notes and references

Electronic Supplementary Information (ESI) available: See DOI: 10.1039/b000000x/

- 1 W. -R. Lee, M. G. Kim, J. -R. Choi, J. -I. Park, S. J. Ko, S. J. Oh and J. Cheon, *J. Am. Chem. Soc.*, 2005, **127**, 16090.
- 2 F. Tao, M. E. Grass, Y. Zhang, D. R. Butcher, J. R. Renzas, Z. Liu, J. Y. Chung, B. S. Mun, M. Salmeron and G. A. Somorjai, *Science*, 2008, **322**, 932.
- 3 Y. W. Lee, M. Kim, Z. H. Kim and A. W. Han, *J. Am. Chem. Soc.*, 2009, **131**, 17036.
- 4 M. Yamauchi, H. Kobayashi and H. Kitagawa, *ChemPhysChem*, 2009, **10**, 2566.
- 5 V. Mazumder, M. Chi, K. L. More and S. Sun, *J. Am. Chem. Soc.*, 2010, **132**, 7848.
- 6 D. Wang, H. L. Xin, Y. Yu, H. Wang, E. Rus, D. A. Muller and H. D. Abruña, *J. Am. Chem. Soc.*, 2010, **132**, 17664.
- 7 A. Sarkar and A. Manthiram, *J. Phys. Chem. C*, 2010, **114**, 4725–4732.
- 8 Y. Chen, Z. Liang, F. Yang, Y. Liu, S. Chen, *J. Phys. Chem. C*, 2011, **115**, 24073.
- 9 B. Lim, J. Wang, P. H. C. Camargo, M. Jiang, M. J. Kim and Y. Xia,

- Nano Lett.*, 2008, **8**, 2535.
- 10 S. I. Sanchez, M. W. Small, J. –M. Zuo and R. G. Nuzzo, *J. Am. Chem. Soc.*, 2009, **131**, 8683.
- 11 J. X. Wang, H. Inada, L. Wu, Y. Zhu, Y. Choi, P. Liu, W. –P. Zhou and R. R. Adzic, *J. Am. Chem. Soc.*, 2009, **131**, 17298.
- 12 K. Sasaki, H. Naohara, Y. Cai, Y. M. Choi, P. Liu, M. B. Vukmirovic, J. X. Wang and R. R. Adzic, *Angew. Chem. Int. Ed.*, 2010, **49**, 8602.
- 13 M. Jiang, B. Lim, J. Tao, P. H. C. Camargo, C. Ma, Y. Zhu and Y. Xia, *Nanoscale*, 2010, **2**, 2406.
- 14 H. Zhang, Y. Yin, Y. Hu, C. Li, P. Wu, S. Wei and C. Cai, *J. Phys. Chem. C*, 2010, **114**, 11861.
- 15 H. Zhang, M. Jin, J. Wang, M. J. Kim D. Yang and Y. Xia, *J. Am. Chem. Soc.*, 2011, **133**, 10422.
- 16 F. Taufany, C. –J. Pan, J. Rick, H. –L. Chou, M. –C. Tsai, B. –J. Hwang, D. –G. Liu, J. –F. Lee, M. –T. Tang, Y. –C. Lee and C. –I. Chen, *ACS Nano*, 2011, **5**, 9370.
- 17 J. W. Hong, S. W. Kang, B. –S. Choi, D. Kim, S. B. Lee and S. W. Han, *ACS Nano*, 2012, **6**, 2410.
- 18 H. Zhang, M. Jin and Y. Xia, *Chem. Soc. Rev.*, 2012, **41**, 8035.
- 19 M. J. Weber, A. J. M. Mackus, M. A. Verheijen, C. van der Marel and W. M. M. Kessels, *Chem. Mater.*, 2012, **24**, 2973.
- 20 R. Choi, S. –I. Choi, C. H. Choi, K. M. Nam, S. I. Woo, J. T. Park and S. W. Han, *Chem. Eur. J.*, 2013, **19**, 8190.
- 21 Y. Li, Y. Wu and B. S. Ong, *J. Am. Chem. Soc.*, 2005, **127**, 3266.

- 22 S. Magdassi, M. Grouchko, O. Berezin and A. Kamyshny, *ACS Nano*, 2010, **4**, 1943.
- 23 Z. Zhang, X. Zhang, Z. Xin, M. Deng, Y. Wen and Y. Song, *Nanotechnology*, 2011, **22**, 425601.
- 24 M. Tsuji, S. Hikino, Y. Sano and M. Horigome, *Chem. Lett.*, 2009, **38**, 518.
- 25 M. Grouchko, A. Kamyshny and S. Magdassi, *J. Mater. Chem.*, 2009, **19**, 3057.
- 26 V. Mancier, C. Rouse-Bertrand, J. Dille, J. Michel and P. Fricoteaux, *Ultrason. Sonochem.*, 2010, **17**, 690.
- 27 J. Zhao, D. Zhang and J. Zhao, *J. Solid State Chem.*, 2011, **184**, 2339.
- 28 Z. Chen, D. Mochizuki, M. M. Maitani and Y. Wada, *Nanotechnology*, 2013, **24**, 265602.
- 29 R. Gedye, F. Smith, K. Westaway, H. Ali, L. Baldisera, L. Laberge and J. Rousell, *Tetrahedron Lett.*, 1986, **27**, 279.
- 30 S. Caddick, *Tetrahedron*, 1995, **51**, 10403.
- 31 S. A. Galema, *Chem. Soc. Rev.*, 1997, **26**, 233.
- 32 R. S. Varma, *Green Chem.*, 1999, **1**, 43.
- 33 K. J. Rao, B. Vaidhyanathan, M. Ganguli and P. A. Ramakrishnan, *Chem. Mater.*, 1999, **11**, 882.
- 34 P. Lidström, J. Tierney, B. Wathey and J. Westman, *Tetrahedron*, 2001, **57**, 9225.
- 35 C. O. Kappe, *Angew. Chem. Int. Ed.*, 2004, **43**, 6250.
- 36 N. E. Leadbeater, *Chem. Commun.*, 2005, **23**, 2881.

- 37 D. Dallinger and C. O. Kappe, *Chem. Rev.*, 2007, **107**, 2563.
- 38 I. Bilecka and M. Niederberger, *Nanoscale*, 2010, **2**, 1358.
- 39 M. N. Nadagouda, T. F. Speth and R. S. Varma, *Acc. Chem. Res.*, 2011, **44**, 469.
- 40 M. Baghbanzadeh, L. Carbone, P. D. Cozzoli and C. O. Kappe, *Angew. Chem. Int. Ed.*, 2011, **50**, 11312.
- 41 M. Nishioka, M. Miyakawa, H. Kataoka, H. Koda, K. Sato and T. M. Suzuki, *Nanoscale*, 2011, **3**, 2621.
- 42 M. Nishioka, M. Miyakawa, H. Kataoka, H. Koda, K. Sato and T. M. Suzuki, *Chem. Lett.*, 2011, **40**, 1204.
- 43 M. Nishioka, M. Miyakawa, Y. Daino, H. Kataoka, H. Koda, K. Sato and T. M. Suzuki, *Ind. Eng. Chem. Res.*, 2013, **52**, 4683.
- 44 B. -J. Hwang, L. S. Sarma, C. -H. Chen, C. Bock, F. -J. Lai, S. -H. Chang, S. -C. Yen, D. -G. Liu, H. -S. Sheu and J. -F. Lee, *J. Phys. Chem. C*, 2008, **112**, 19922.
- 45 J. -P. Sylvestre, A. V. Kabashin, E. Sacher, M. Meunier and J. H. T. Luong, *J. Am. Chem. Soc.*, 2004, **126**, 7176.
- 46 J. Yang, T. C. Deivaraj, H. -P. Too and J. Y. Lee, *Langmuir*, 2004, **20**, 4241.
- 47 G. W. Slawiński and F. P. Zamborini, *Langmuir*, 2007, **23**, 10357.

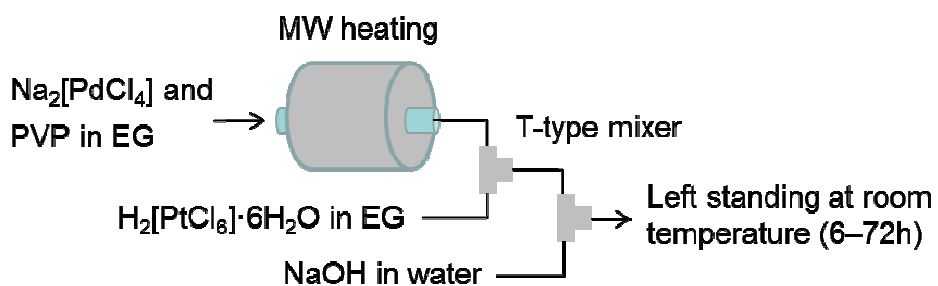


Fig. 1 Schematic showing continuous synthesis of metal@metal core-shell nanoparticles. The Pd nanoparticle dispersion was synthesized from $\text{Na}_2[\text{PdCl}_4]$ by MW heating of the EG solution. It was then transferred directly to Pt shell formation by a galvanic displacement reaction.

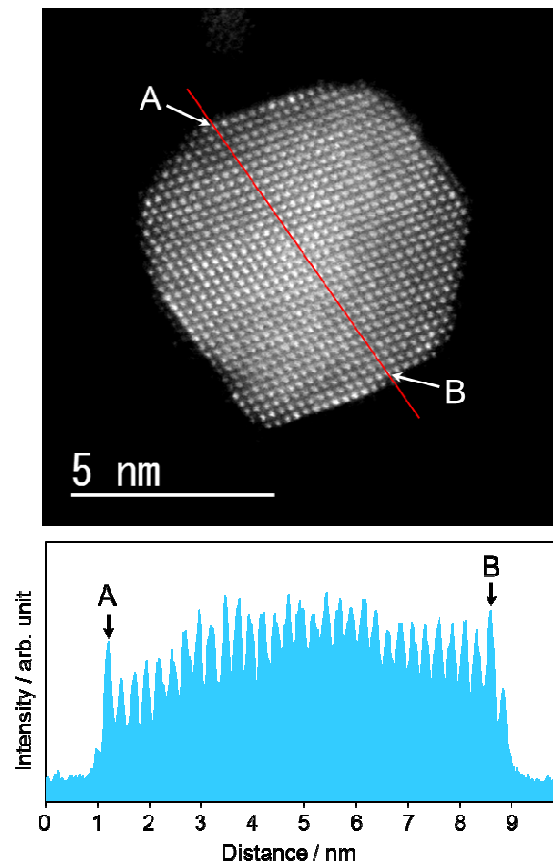


Fig. 2 HAADF-STEM image of Pd@Pt core-shell nanoparticles and the distribution of contrast.

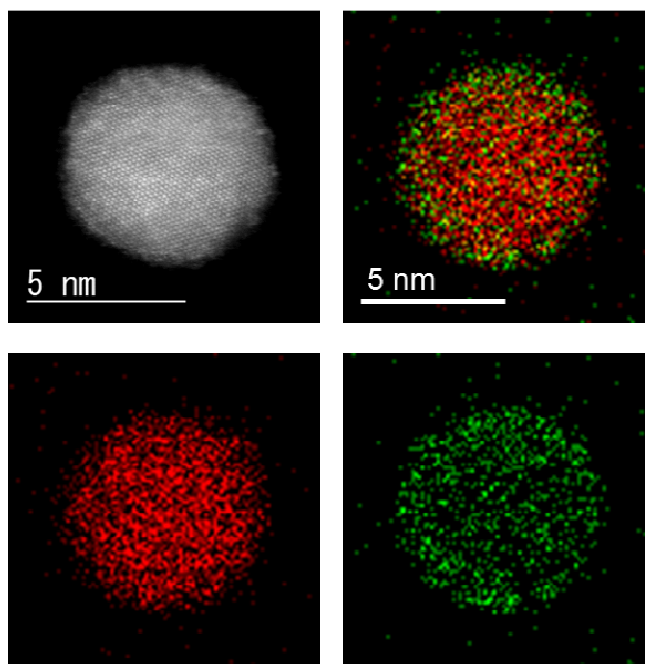


Fig. 3 Elemental mapping images of Pd@Pt core-shell nanoparticles, where Pd and Pt elements are displayed, respectively, as red and green colors.

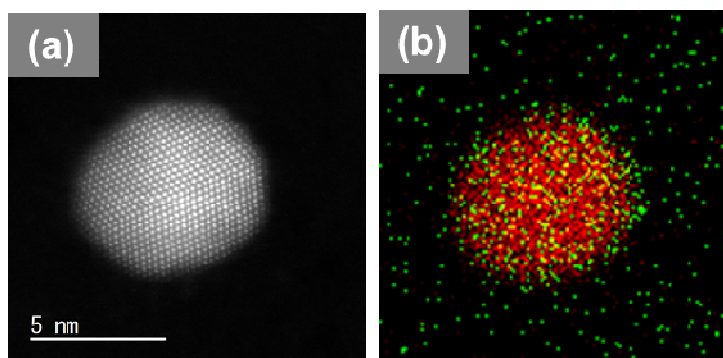


Fig. 4(a) HAADF-STEM image and (b) elemental mapping image of nanoparticles synthesized without pH control. Pd and Pt are shown, respectively, as red and green. The EDS atomic ratio of Pd : Pt was 99 : 1. The Pt shell was formed only slightly on the Pd nanoparticle surface.

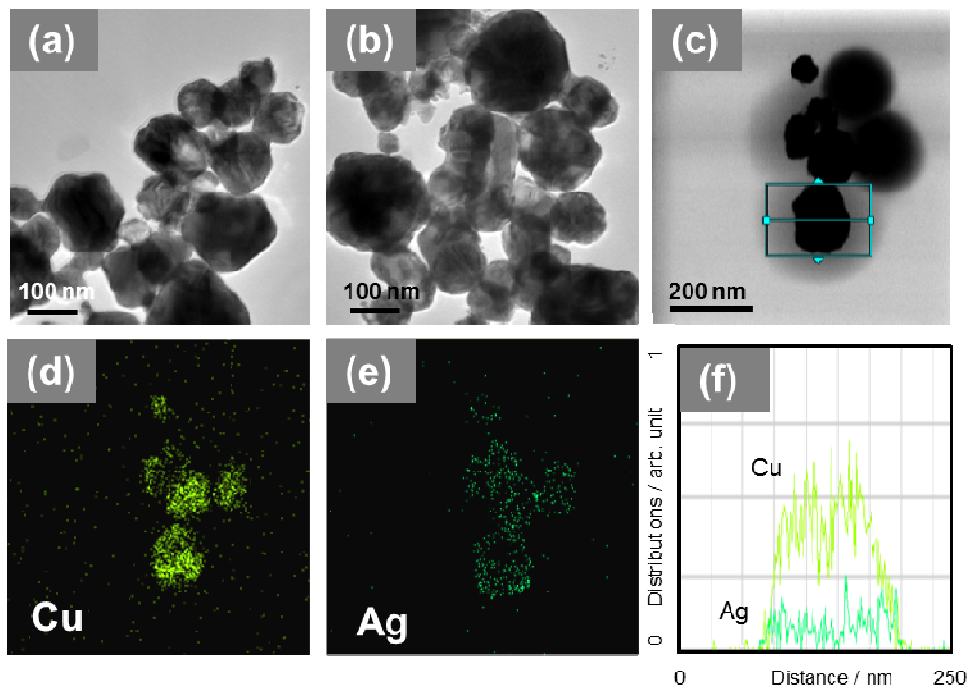


Fig. 5 TEM images and EDS elemental mapping of Cu and Cu@Ag core-shell nanoparticles: (a) TEM image of Cu nanoparticles. (b, c) TEM images of a Cu@Ag core-shell nanoparticle, (d, e) EDS mapping images of Cu and Ag for Cu@Ag core-shell nanoparticles, and (f) distribution of Cu and Ag atoms along the cross section line shown in the TEM image (c).

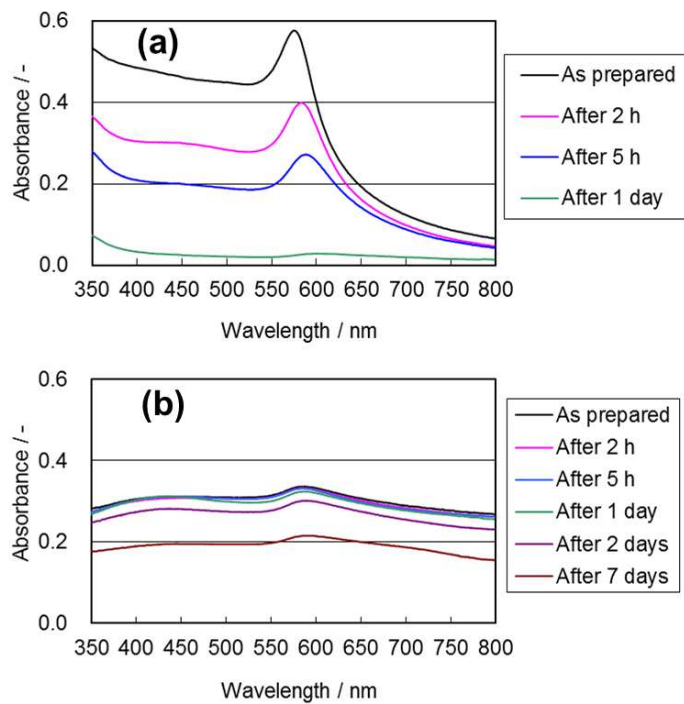
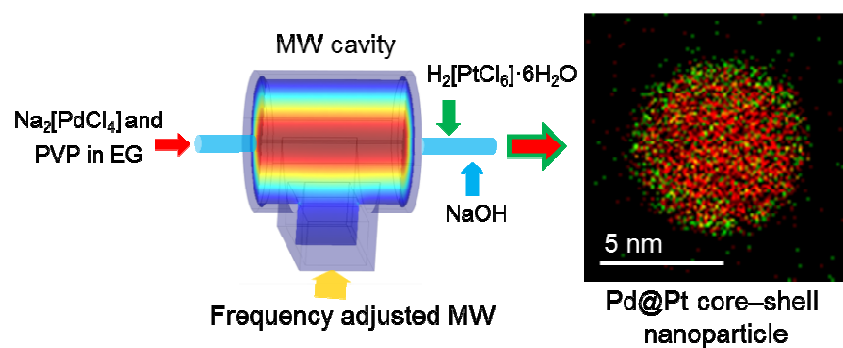


Fig. 6 Time course of UV-vis spectra: (a) Cu nanoparticle dispersion and (b) Cu@Ag core-shell nanoparticle dispersion.

Table of contents



Continuous syntheses of Pd@Pt core-shell nanoparticles were performed using flow processes including microwave-assisted Pd core-nanoparticle formation followed by galvanic displacement with a Pt shell.